# Unravelling the sbottom spin at the CERN LHC

Alexandre Alves[1, *] and Oscar Éboli[1, †]

[1]*Instituto de Física, Universidade de São Paulo, São Paulo, Brazil*
(Dated: **02/04/07**)

Establishing that a signal of new physics is undoubtly supersymmetric requires not only the discovery of the supersymmetric partners but also probing their spins and couplings. We show that the sbottom spin can be probed at the CERN Large Hadron Collider using only angular correlations in the reaction $pp \rightarrow \tilde{b}\tilde{b}^* \rightarrow b\bar{b}\not{p}_T$, which allow us to distinguish a universal extra dimensional interpretation with a fermionic heavy bottom quark from supersymmetry with a bosonic bottom squark. We demonstrate that this channel provides a clear indication of the sbottom spin provided the sbottom production rate and branching ratio into $b\tilde{\chi}_1^0$ are sufficiently large to have a clear signal above Standard Model backgrounds.

## I. INTRODUCTION

Supersymmetric models are promising candidates for physics beyond the Standard Model (SM), despite the present lack of direct experimental evidence on supersymmetry (SUSY). The CERN Large Hadron Collider (LHC) has a large reach for the discovery of SUSY [1] that largely relies on the production and decay of strongly interacting new particles *i.e.* squarks and gluinos [2, 3]. Establishing that a signal of new physics at the LHC is indeed supersymmetric requires not only the discovery of the new supersymmetric partners but also probing their interactions and spins [4, 5, 6, 7].

Previously, the squark spin has been studied through the long decay chain $\tilde{q} \rightarrow \tilde{\chi}_2^0 \rightarrow \tilde{\ell} \rightarrow \tilde{\chi}_1^0$ which is also used to measure its mass [4, 6] or in conjunction with the gluino spin analysis in the decay chain $\tilde{g} \rightarrow \tilde{b} \rightarrow \tilde{\chi}_2^0 \rightarrow \tilde{\ell} \rightarrow \tilde{\chi}_1^0$ [7]. In this work we probe the potential of the CERN Large Hadron Collider (LHC) for unravelling the bottom squark spin using angular correlations in the short decay chain $pp \rightarrow \tilde{b}\tilde{b}^* \rightarrow b\bar{b}\not{p}_T$, analogously to what has been done for the analysis of the slepton spin [4, 5]. A nice feature of this reaction is that only sbottoms and the lightest SUSY particle (LSP) takes place in it, providing a further check of sbottom spin obtained in the long decay chain studies. Unfortunately, this analysis can not be extended straightforwardly to light flavor squarks due to large QCD backgrounds.

To determine the spin nature of the sbottoms at the LHC we compare the SUSY sbottom production and decay chain with another scenario where the new intermediate states have the same spin as the SM particles and leads to the same final state $b\bar{b}\not{p}_T$. Such a model are Universal Extra Dimensions (UED) [8] where each SM particle has a heavy Kaluza–Klein (KK) partner which can mimic the SUSY cascade decay, provided we employ the mass spectra extracted from the decay kinematics match [9]. Here we are not focusing on UED searches but we use UED only for comparison with the SUSY predictions.

There are many observables which we can use to discriminate 'typical' UED and SUSY models, like the production rate or the mass spectrum. Nevertheless, at the LHC we measure only production cross sections times branching ratios, and the UED as well as the SUSY mass spectra are unlikely to be what we currently consider 'typical'. On the other hand, spin information is generally extracted from angular correlations. Therefore, we base our analysis exclusively on distributions of the outgoing SM $b$ quarks as predicted by UED and by SUSY. We demonstrate that this final state $b\bar{b}\not{p}_T$ provides a clear indication of the sbottom spin provided the sbottom production rate and branching ratio into $b\tilde{\chi}_1^0$ are sufficiently large to have a clear signal above SM backgrounds.

---

*Electronic address: aalves@fma.if.usp.br
†Electronic address: eboli@fma.if.usp.br

## II.  UED INTERACTIONS AND PARAMETERS

We assumed one extra dimension with size $R$, where all SM fields propagate [8, 9], leading to a tower of discrete KK excitations for each of the SM fields ($n = 0$). In this scenario, the 5-dimensional wave functions for an SU(2)–doublet fermion are

$$\psi_d = \frac{1}{\sqrt{2\pi R}}\psi_{dL}^{(0)} + \frac{1}{\sqrt{\pi R}}\sum_{n=1}^{\infty}\left(\psi_{dL}^{(n)}\cos\frac{ny}{R} + \psi_{dR}^{(n)}\sin\frac{ny}{R}\right) \ . \tag{1}$$

On the other hand, the roles of the left and right handed $n$-th KK excitations are reversed for SU(2) singlets. Just like in the MSSM, the spinors of the singlet ($q$) and doublet ($Q$) KK–fermion mass eigenstates can be expressed in terms of the SU(2) doublet and singlet fields $\psi_{d,s}$

$$\begin{aligned}
Q^{(n)} &= \cos\alpha^{(n)}\psi_d^{(n)} + \sin\alpha^{(n)}\psi_s^{(n)} \ , \\
q^{(n)} &= \sin\alpha^{(n)}\gamma^5\psi_d^{(n)} - \cos\alpha^{(n)}\gamma^5\psi_s^{(n)} \ .
\end{aligned} \tag{2}$$

In general, the mixing angle $\alpha^{(n)}$ is suppressed by the SM fermion mass over the KK–excitation mass plus one–loop corrections except for the top quark due to its large mass.

$$\tan 2\alpha^{(n)} = \frac{m_f}{\frac{n}{R} + \frac{1}{2}(\delta m_Q^{(n)} + \delta m_q^{(n)})} \tag{3}$$

The non–degenerate KK–mass terms $\delta m^{(n)}$ contain tree level and loop contributions to the KK masses, including possibly large contributions from non–universal boundary conditions.

The neutral KK gauge fields will play the role of neutralinos in the alternative description of the sbottom production and decay. Just as in the SM, there is a KK–weak mixing angle which for each $n$ rotates the interaction eigenstates into mass eigenstates

$$\begin{aligned}
\gamma_\mu^{(n)} &= \cos\theta_w^{(n)}\, B_\mu^{(n)} + \sin\theta_w^{(n)}\, W_{3,\mu}^{(n)} \ , \\
Z_\mu^{(n)} &= -\sin\theta_w^{(n)}\, B_\mu^{(n)} + \cos\theta_w^{(n)}\, W_{3,\mu}^{(n)} \ .
\end{aligned} \tag{4}$$

The $n$-th KK weak mixing angle is again mass suppressed

$$\tan 2\theta_w^{(n)} = \frac{v^2\, g\, g_Y/2}{(\delta m_{W_3}^{(n)})^2 - (\delta m_B^{(n)})^2 + v^2\,(g^2 - g_Y^2)/4} \tag{5}$$

where $\delta m^{(n)}$ contains tree level as well as loop corrections to the KK gauge boson masses. Generally $(\delta m_{W_3}^{(n)})^2 - (\delta m_B^{(n)})^2 \gg v^2\,(g^2 - g_Y^2)$ [9] and the lightest KK partner is the $B^{(1)}$, with basically no admixture from the heavy $W_3^{(1)}$.

We only considered the first set of KK excitations to formulate an alternative interpretation of production and decay of sbottoms at the LHC, using the UED decay $b^{(1)} \rightarrow b\gamma^{(1)}$ to mimic a sbottom decay. The relevant interactions for this decay are

$$\mathcal{L}_{\gamma_1 q_1 q} = ig_Y\left[\,\bar{q}^{(0)}\gamma^\mu\left(Y_d\cos\alpha^{(1)}P_L + Y_s\sin\alpha^{(1)}P_R\right)Q^{(1)} - \bar{q}^{(0)}\gamma^\mu\left(Y_d\sin\alpha^{(1)}P_L + Y_s\cos\alpha^{(1)}P_R\right)q^{(1)}\right]\gamma_\mu^{(1)} \ . \tag{6}$$

In general, the KK partners of the SM particles do not have a mass spectrum similar to what we expect in SUSY, however, we imposed that the first KK excitations have the same mass as the SUSY particles. Assigning the LSP mass to the Lightest KK Particle (LKP) and the Next-LSP mass to the Next-LKP mass fixes the KK-weak mixing angle by means of Eq. (5)

$$\theta_w^{(1)} = \frac{1}{2}\arctan\left(\frac{gg_Y v^2}{2(m_{NLSP}^2 - m_{LSP}^2)}\right) \ . \tag{7}$$

| test point | particle | mass (GeV) | branching ratio |
|------------|----------|------------|-----------------|
| S5 | $\tilde{\chi}_1^0$ | 122. | stable |
| S5 | $\tilde{b}_1$ | 633. | $\mathrm{Br}(\tilde{b}_1 \to b\tilde{\chi}_1^0) = 26.6\%$ |
| S5 | $\tilde{b}_2$ | 663. | $\mathrm{Br}(\tilde{b}_2 \to b\tilde{\chi}_1^0) = 78.8\%$ |
| SPS1a | $\tilde{\chi}_1^0$ | 97. | stable |
| SPS1a | $\tilde{b}_1$ | 517. | $\mathrm{Br}(\tilde{b}_1 \to b\tilde{\chi}_1^0) = 4.4\%$ |
| SPS1a | $\tilde{b}_2$ | 547. | $\mathrm{Br}(\tilde{b}_2 \to b\tilde{\chi}_1^0) = 29\%$ |
| L1 | $\tilde{\chi}_1^0$ | 97.8 | stable |
| L1 | $\tilde{b}_1$ | 280. | $\mathrm{Br}(\tilde{b}_1 \to b\tilde{\chi}_1^0) = 40\%$ |
| L1 | $\tilde{b}_2$ | 354. | $\mathrm{Br}(\tilde{b}_2 \to b\tilde{\chi}_1^0) = 20\%$ |

Table I: Masses of sbottoms, the lightest neutralino, and branching ratios of $\tilde{b}_{1,2} \to b\tilde{\chi}_1^0$ for the test points considered in our numerical simulations.

## III.   EVENT SIMULATION AND TEST POINTS

We considered three scenarios for the new particle spectrum. Our first test point is the LHC point 5 (S5) [10] that exhibits rather heavy sbottoms with sizeable decays into $b\tilde{\chi}_1^0$; see Table I. Our second reference point is SPS1a [11] where the sbottom masses are close to ones in the first scenario, however the decays $\tilde{b}_{1,2} \to b\tilde{\chi}_1^0$ are suppressed. The third test point exhibits a somewhat light squark spectrum which could be eventually produced at a 1 TeV International $e^+e^-$ Linear Collider; we denote this point by L1. The masses for the L1 parameter point are $m_{\tilde{b}_1} = 280$ GeV, $m_{\tilde{b}_2} = 354$ GeV, $m_{\tilde{t}_1} = 339$ GeV, $m_{\tilde{t}_2} = 371$ GeV, and $m_{\tilde{\chi}_1^0} = 97.8$ GeV. For the SPS1a and S5 parameter choices the lighter of the two sbottoms is almost entirely a left state $\tilde{b}_1 \sim \tilde{b}_L$ while for L1 it is approximately a maximal mixture of left and right states $\tilde{b}_1 \sim \sqrt{2}/2\tilde{b}_L + \sqrt{2}/2\tilde{b}_R$. The salient features of these reference points is summarized in Table I.

In order to correctly treat all spin correlations we performed a parton–level analysis including the UED interactions in MADGRAPH [12] and using SMADGRAPH [13] for the SUSY simulation. In our calculations we used CTEQ6L1 parton distribution functions [14] with the factorization and renormalization scales are fixed by $\mu_F = \mu_R = (m_{\tilde{b}_1} + m_{\tilde{b}_2})/2$ for the signal and $\mu_F = \mu_R = m_V + \sum_i \mathrm{p}_{T_i}$ for the SM backgrounds, where $m_V$ is the mass of the relevant electroweak gauge boson and $\sum_i \mathrm{p}_{T_i}$ is the sum of the transverse momentum of additional jets.

We simulated experimental resolutions by smearing the energies (but not directions) of all final state partons with a Gaussian error. We considered a jet resolution $\Delta E/E = 0.5/\sqrt{E} \oplus 0.03$ and $\sigma_{E_T} = 0.46\sqrt{\sum E_T}$ for the missing transverse energy where $\sum E_T$ is the sum of the jet transverse energies. In addition to that we included a b-tagging efficiency of $\varepsilon = 60\%$ with a mistagging probability of $1/200$ for light jets [15]. No K-factors were applied to signals or backgrounds since we do not expect QCD corrections to change significantly the shape of kinematical distributions [2, 3]. Nevertheless, given the increasing interest in studying spins correlations at the LHC by means of long and short decay chains, it is important to check if this is indeed the case.

## IV.   ANALYSIS AND RESULTS

At the LHC we analyzed the production of sbottom pairs followed by their decay in a $b$ and the LSP

$$pp \to \tilde{b}_{1,2}\tilde{b}_{1,2}^* \to b\bar{b}\tilde{\chi}_1^0\tilde{\chi}_1^0 \to b\bar{b}\slashed{p}_T \ , \tag{8}$$

*i.e.* the signal is characterized by two b-tagged jets and missing transverse energy. One feature of the reaction (8) is that the s–channel subprocesses $q\bar{q} \to \tilde{b}\tilde{b}^*$ present the well–known angular distribution

$$\frac{d\sigma}{d\cos\theta^*} \propto 1 - \cos^2\theta^* \tag{9}$$

where $\theta^*$ is the polar angle of produced scalar particles in their center-of-mass frame. However, this clean signature of the sbottom spin is contaminated by the subprocess $gg \to \tilde{b}\tilde{b}^*$ which contains $t$-channel diagrams and quartic couplings; see Fig. 1 left panel. Therefore, it is easier to decipher the new state spin if we enhance the importance of the $q\bar{q}$ s–channel subprocesses via a judicious choice of cuts. Notwithstanding, the cuts to isolate the signal must not introduce bias in the angular distributions used to study the sbottom spin.
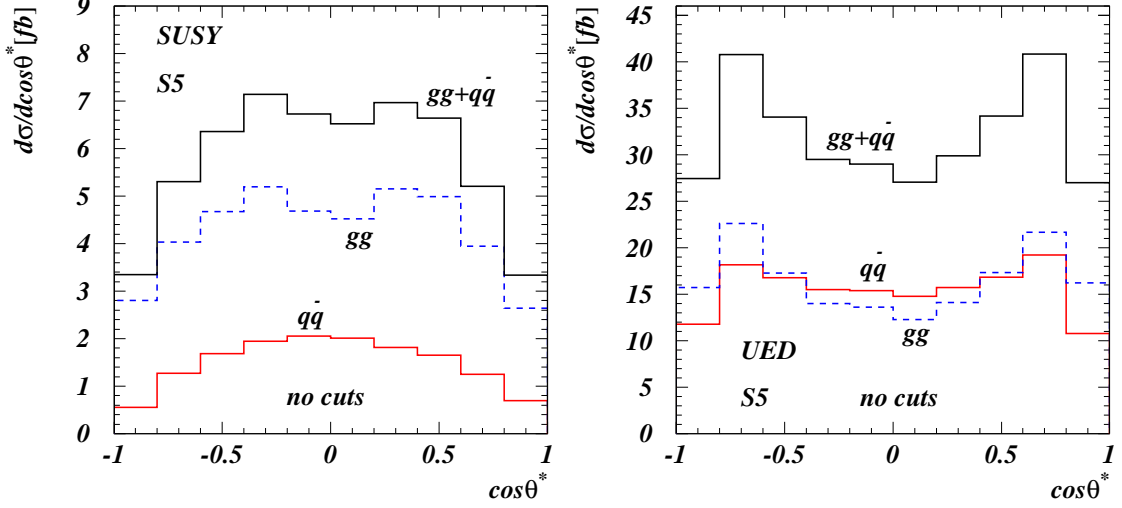
Figure 1: Left panel: $\cos\theta^*$ distribution for the production of sbottoms coming from $q\bar{q}$ and $gg$ fusions. Right panel: same distribution as in the right panel but for the production of $b^{(1)}$. We used the test point S5 spectrum.

On the other hand, the center–of–mass angular distribution of KK bottoms in UED produced by $q\bar{q}$ fusion is

$$\frac{d\sigma}{d\cos\theta^*} \propto 1 + \left(\frac{E_{b_1}^2 - m_{b_1}^2}{E_{b_1}^2 + m_{b_1}^2}\right)\cos^2\theta^* , \qquad (10)$$

where $M_{b_1}$ and $E_{b_1}$ are the mass and energy respectively of the $b^{(1)}$ in the center–of–mass frame. This distribution peaks in the forward and backward directions being quite distinct of the SUSY prediction. Moreover, we must also include the $gg \to b^{(1)}\bar{b}^{(1)}$ which contains t- and s-channel contributions which present a peak towards the forward and backward regions as well; see Fig. 2 right panel.

At the LHC we can not reconstruct the the polar angle ($\theta^*$) of produced particles in their center-of-mass frame due to the presence of undetected $\tilde{\chi}_1^0$ or $\gamma^{(1)}$. Therefore, we must use an alternative variable that retains part of the information carried by $\theta^*$. A convenient variable to use in our analysis is [5]

$$\cos\theta_{bb}^* \equiv \tanh\left(\frac{\Delta\eta_{bb}}{2}\right) \qquad (11)$$

where $\Delta\eta_{bb}$ is the rapidity separation of the $b$-tagged jets. Notice that $\Delta\eta_{bb}$ is invariant under boosts along the collision axis, and consequently, $\cos\theta_{bb}^*$ is invariant under boosts as well. The angle $\theta_{bb}^*$ is the polar angle between each reconstructed bottom jet direction in the longitudinally boosted frame in which the rapidities of the bottoms are equal and opposite.

In order to $\cos\theta_{bb}^*$ carry information of the produced particle spin, the flight directions of sbottoms and bottoms must be correlated. We depict in the left panel of Fig. 2 the cosine of the opening angle between the bottom and the sbottom flight directions in the $\tilde{b}\tilde{b}^*$ center–of–mass system for the S5 and L1 spectra. Clearly, the bulk of the signal is concentrated in region of small opening angles as a consequence of the large energy of the sbottoms after cuts.

Fig. 3 shows that $\cos\theta_{bb}^*$ is indeed strongly correlated to the cosine of production polar angle ($\theta^*$) of the sbottoms and $b^{(1)}$'s in their center–of–mass system. Therefore, we must expect the shape of $\cos\theta_{bb}^*$ distributions to resemble the polar angle spectra of sbottoms and KK bottoms apart from some smearing effects due to non-perfect correlations between the bottoms and sbottoms (KK bottoms) flight directions. Nevertheless, a clear separation between SUSY and UED distributions should be possible as was demonstrated in the case of smuon pair production at the LHC [5]. Taking a closer look at Fig. 3 we already realize that UED events are slightly more concentrated near $\cos\theta_{bb}^* = \pm 1$ while SUSY events are homogeneously distributed along the direction $\cos\theta_{bb}^* = \cos\theta_{\tilde{b}}$.

In our analysis, we included the following backgrounds for the process $pp \to b\bar{b}\not{p}_T$:

- SM QCD and electroweak production of $b\bar{b}Z$ with $Z \to \nu\bar{\nu}$ that accounts for $\simeq 91\%$ of the total background after cuts for the S5 and SPS1a test points and $\simeq 72\%$ for the L1 scenario.
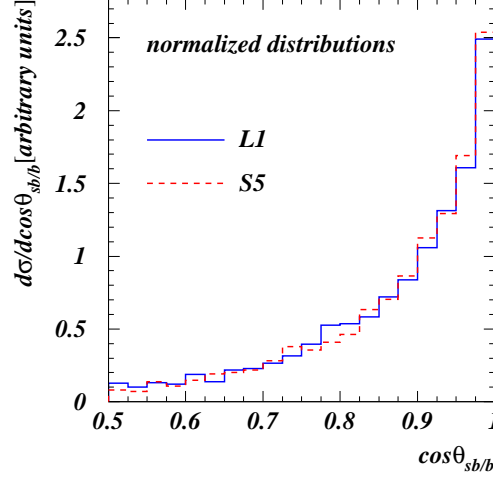
Figure 2: Cosine of the opening angle between the bottom and the sbottom in center–of–mass system for two different mass spectra considered here.
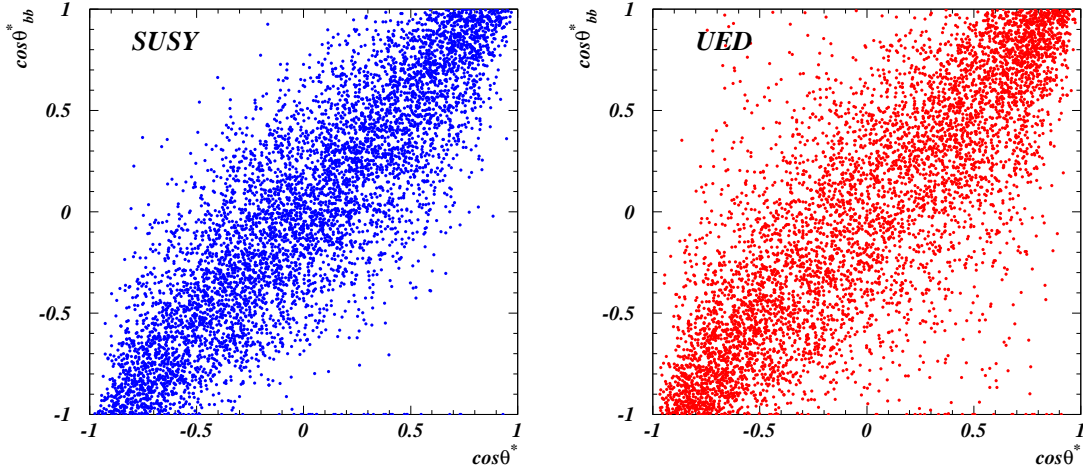


Figure 3: In the left (right) panel we display a scattered plot $\cos\theta^*_{bb} \otimes \cos\theta^*$ for sbottoms ($b^{(1)}$) production. Here we chose the parameter point S5.

- Reducible electroweak and QCD backgrounds like $jjZ$, $jjW$, $j\tau\nu_\tau$, $b\bar{b}j$, $jj$, $jjj$, and $jjb$ where some of the decay products evade detection and $j$ stands for a light jet that might be mistagged as a $b$ jet. These dangerous backgrounds are efficiently reduced by the requirement of two $b$-tagged jets. The second largest background after cuts is $bbW$ where the lepton from the W boson has a large rapidity $|\eta_\ell| > 2.5$.

- SUSY processes, excluding $\tilde{b}\tilde{b}^*$ production, that lead to the final state $b\bar{b}\tilde{\chi}^0_1\tilde{\chi}^0_1$.

In order to properly trigger [16] the event and tag the b-jets [15] the following acceptance cuts were imposed in all cases

$$|\eta_b| < 2.5 \quad , \quad p_T^b > 100 \text{ GeV} \quad , \quad \Delta R_{bb} > 0.7 \quad , \quad \not{p}_T > 100 \quad . \tag{12}$$

A potentially large background is the QCD production of dijets once we take into account that mismeasurements of the jets properties can lead to missing transverse momentum and that this process has a huge cross section. This background can be efficiently reduced by the missing transverse momentum cut Eq. (12) and by requiring that the

azimuthal angle between the jets and the missing transverse momentum satisfy

$$|\Delta\Phi(\not{p}_T, p_{Tj})| > 0.3 \quad . \tag{13}$$

In the L1 test point simulations we applied the following cuts not only to enhance the signal and deplete the background but also to augment the importance of the $q\bar{q}$ s-channel subprocess

$$M_{b\bar{b}} > 300 \text{ GeV} \quad , \quad M_{\text{eff}} > 600 \text{ GeV} \quad , \quad |\Delta\Phi(\not{p}_T, p_{Tj_{soft}})| < 2.4 \quad , \tag{14}$$

where $M_{\text{eff}}$ is the sum of all jet and missing transverse momenta and $\Delta\Phi(\not{p}_T, p_{Tj_{soft}})$ the azimuthal angle between the missing transverse momentum and the softest jet. After cuts the SUSY signal cross section is 38.1 fb while the background cross section is 2.4 fb, leading to $S/B \simeq 16.6$.

For the parameter point S5 we used the following cuts to optimize the signal

$$M_{b\bar{b}} > 600 \text{ GeV} \quad , \quad M_{\text{eff}} > 1 \text{ TeV} \quad , \quad |\Delta\Phi(\not{p}_T, p_{Tj_{soft}})| < 2.4 \quad . \tag{15}$$

The SUSY signal cross section at this test point is 4.55 fb with a background of 1.24 fb and $S/B \simeq 3.7$ while the $q\bar{q}$ fusion accounts for $\simeq 40\%$ of the signal events. On the other hand, $\simeq 45\%$ of the UED signal stems from $q\bar{q}$ fusion. The cuts employed in this case were harder for two reasons: first, the bottoms are harder in this case once the sbottom is much heavier than the neutralino compared to L1 case; second, the signal cross section is significantly smaller than in the L1 case which required a deeper suppression of backgrounds to avoid a severe bias on the signal angular distributions.

Finally, we imposed the following cuts for the test point SPS1a

$$M_{b\bar{b}} > 600 \text{ GeV} \quad , \quad M_{\text{eff}} > 1 \text{ TeV} \quad , \tag{16}$$

which lead to a signal (background) cross section of 1.07 (1.46) fb and $S/B \simeq 0.73$.

In the left panel of Fig. 4 we show the impact of cuts on the $d\sigma/d\cos\theta^*_{bb}$ distributions for SUSY and UED predictions assuming the S5 spectrum. We normalized the UED signal cross section to the SUSY one. As the background events populate the bins of larger $|\cos\theta^*_{bb}|$, the selection cuts tend to suppress that region enhancing the central region for both SUSY and UED. The variable $\Delta\Phi(\not{p}_T, p_{Tj})$ is efficient in rejecting dangerous SM backgrounds like dijet production, however, it has a potential to bias the distributions as we can see in the left panel of Fig. 4. Therefore, a harder cut on this variable is not recommended in the study of spin correlations.

A natural question at this point is whether we can mimic the SUSY signal by varying the UED mixing angles. According to Section II there is not very much room to modify the UED Lagrangian to bring kinematical correlations closer to the SUSY prediction. The KK weak mixing angle $\theta_w^{(n)}$ in Eq. (5) is fixed by the KK masses, so we can not change it while keeping the masses fixed. The same limitations hold when we try to adjust the mixing between the singlet and doublet KK fermions, described by the angle $\alpha^{(n)}$; see Eq. (2). In contrast to the 3rd–generation sfermion sector in the MSSM, the UED mixing angle is not a (third) free parameter, even if we move around the masses invoking boundary conditions. Notwithstanding, for illustration purpose we vary $\alpha^{(1)}$ in the right panel Fig. 4 to check whether the SUSY $\cos\theta^*_{bb}$ can be reproduced by a UED decay chain with different couplings to the fermions. From Eq. (6) we see that varying $\alpha^{(1)}$ effectively enhances the left or right couplings of the KK bottom decay into bottom plus LKP. This figure allows us to see that the changes in the UED parameters are not sufficient to mimic the SUSY predictions.

We depict in Fig. 5 the $\cos\theta^*_{bb}$ spectrum with/without adding the background for the S5 test point, an integrated luminosity of 300 fb$^{-1}$, and after applying cuts (12) and (15). To avoid using any information but the spin we assume the S5 spectrum for the UED particles and normalize their production cross section times branching fractions to the SUSY rate. From Figure 5, we can easily see that the production of fermionic strongly interacting states (UED) favor large separations ($\cos\theta^*_{bb}$) between the $b$-tagged jets while the production of scalar particles (SUSY) leads to a rather constant distribution. Note that these distributions indeed resembles the distributions of the production angles in the center–of–mass system which reflects the correlation between these observables. Moreover, the UED $\cos\theta^*_{bb}$ distribution is similar to the SM background one since they take place through similar diagrams containing KK partners or SM particles with the same spin quantum numbers.

For the assumed integrated luminosity it is rather easy to distinguish between the two models. These two possibilities can be disentangled, for instance, through the asymmetry:

$$A = \frac{\sigma(|\cos\theta^*_{bb}| < 0.5) - \sigma(|\cos\theta^*_{bb}| > 0.5)}{\sigma(|\cos\theta^*_{bb}| < 0.5) + \sigma(|\cos\theta^*_{bb}| > 0.5)} \; . \tag{17}$$
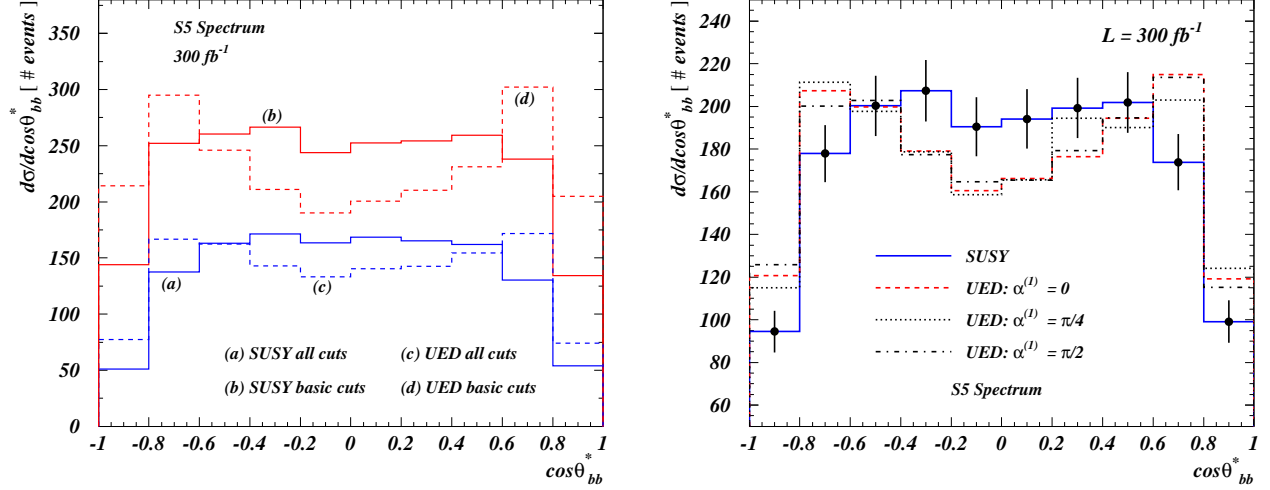
Figure 4: Left panel: impact of cuts on the $d\sigma/d\cos\theta^*_{bb}$ distributions for SUSY and UED signals. We normalized the UED signal cross sections to the SUSY ones using the S5 spectrum. Right panel: SUSY and UED $d\sigma/d\cos\theta^*_{bb}$ distributions without backgrounds but varying the KK bottom mixing angle $\alpha^{(1)}$. The basic cuts are the acceptance defined in Eq. (12) plus $M_{b\bar{b}} > 600$ GeV.
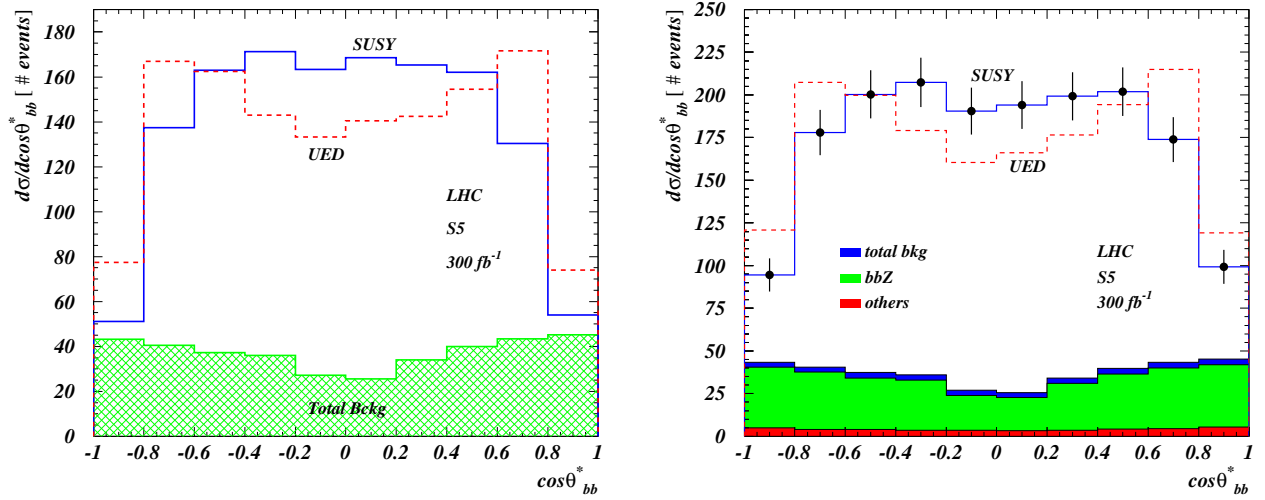


Figure 5: In the left (right) panel we plot the $\cos\theta^*_{bb}$ distribution without (with) the addition of the background contribution. Here we used the parameter point S5 and assumed an integrated luminosity of 300 fb$^{-1}$. The error bars indicate the expected statistical uncertainties.

This asymmetry is $+0.238 \pm 0.023$ for the UED spin assignment while the SUSY interpretation it is significantly larger $+0.373 \pm 0.022$ where the quoted errors are statistical. We estimate that an integrated luminosity of 300 fb$^{-1}$ is needed to reach a $5\sigma$ level signal for the S5 spectrum.

The determination of the sbottom spin is much easier for the test point L1 due to the large $\tilde{b} \to b\tilde{\chi}^0_1$ branching ratio and production cross section. We depicted in Fig. 6 the $\cos\theta^*_{bb}$ distribution and without/with adding the SM background. In this case a mere integrated luminosity of 15 fb$^{-1}$ is enough to discriminate at the $5\sigma$ level UED and SUSY. The asymmetries are given by $+0.565 \pm 0.019$ for SUSY and $+0.365 \pm 0.021$ for UED for this integrated luminosity. Therefore, there is a clear distinction between the two spin assignments (UED $\times$ SUSY) for both S5 and L1 mass spectra and the above integrated luminosities.

The results for the reference point SPS1a are quite different from the S5 and L1 ones. Due to small $\tilde{b} \to b\tilde{\chi}^0_1$ branching ratio, the SM backgrounds play a major role. We can see in the left panel of Fig. 7 that the pure SUSY and UED $\cos\theta^*_{bb}$ spectrum are quite different. However, once we add the SM background, which has a shape similar to UED, it is no longer easy to separate the SUSY from UED, even for an integrated luminosity of 1 ab$^{-1}$; see the
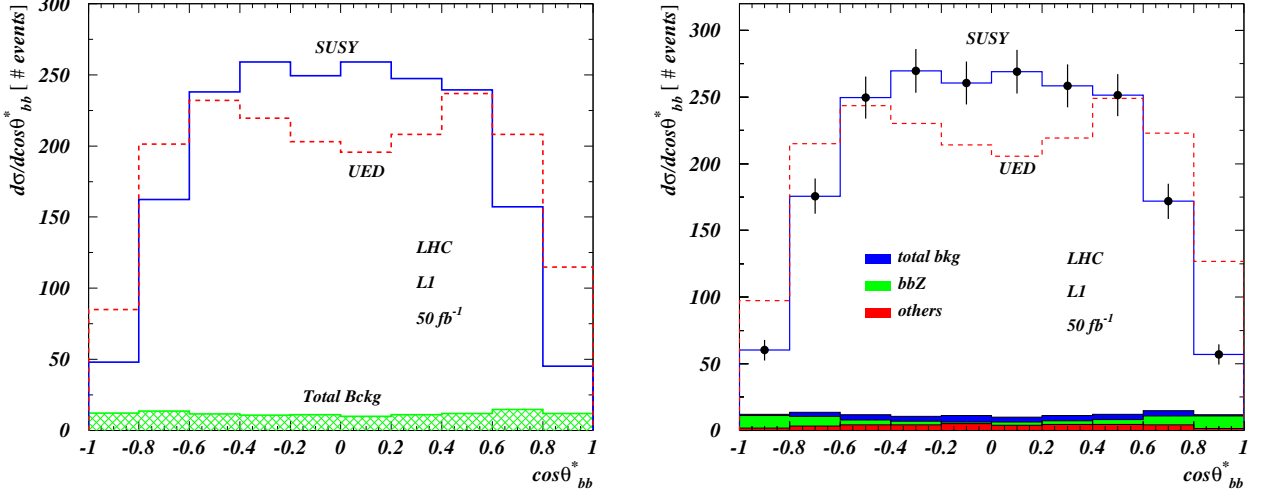
Figure 6: Same as Fig. 5 but for the parameter point L1 and an integrated luminosity of 50 fb$^{-1}$.
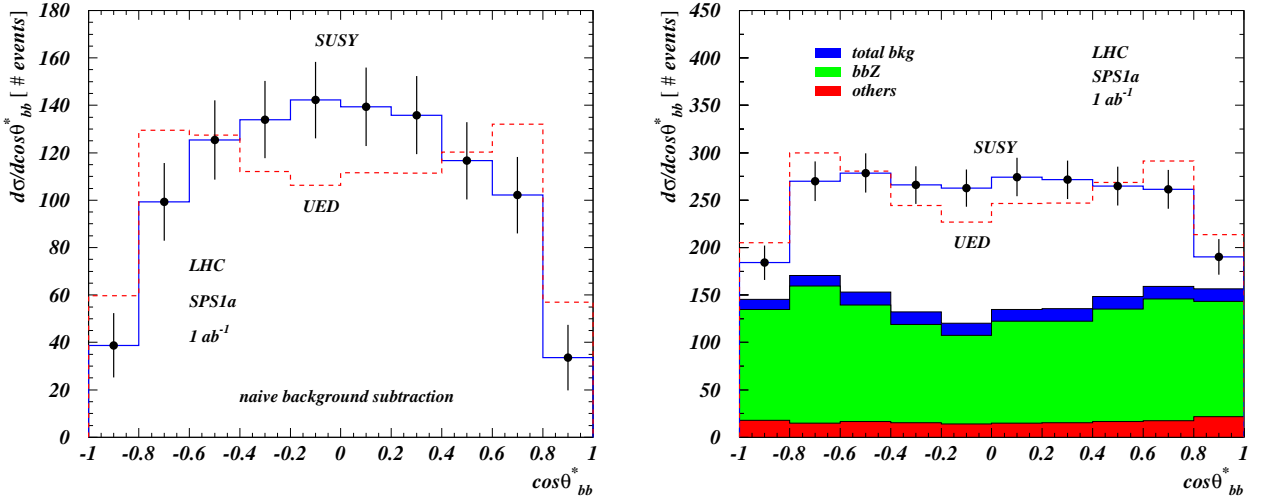


Figure 7: Same as Fig. 5 but for the parameter point SPS1a and an integrated luminosity of 1 ab$^{-1}$.

right panel of Fig. 7. For instance, the asymmetry (17) is $0.282 \pm 0.019$ for SUSY and $0.200 \pm 0.019$ for UED and this extremely large luminosity. In this case SUSY and UED can be discriminated only at at $\sim 4\sigma$ level. Therefore, it is important for this point to subtract the SM background which can be estimated, for instance, from the measurement of the $b\bar{b}\mu^+\mu^-$ cross section. If we neglect systematic errors associated to this extraction from data, the sbottom spin can be determined at $5\sigma$ level for an integrated luminosity of $\simeq 500$ fb$^{-1}$. The left panel of Fig. 7 displays the distributions of SUSY and UED after a naive background subtraction where we just did not add the background to the signals and the error bars calculated as $\sqrt{S + B}$. A dedicated study is necessary to determine the actual impact of the statistical and systematic errors [17].

In general, we noticed that the expected shape of distributions in $\cos\theta^*_{bb}$ are similar to the ones in smuon pair production and decay to $\mu\chi^0_1$ [5], which shows the universality and robustness of the method. Moreover, in both cases ($\tilde{b}^*sbx$ and $\tilde{\mu}^*\tilde{\mu}$) the S5 spectrum seems to be more promising as compared to the SPS1a spectrum, for example, SUSY *versus* UED discrimination of smuon spin assignments is possible in the case of S5 (SPS1a) for an integrated luminosity of 200 fb$^{-1}$(500 fb$^{-1}$).

As a final remark note that, apart from negligible effects from $b\bar{b}$ initiated contributions which include interactions with gluinos and electroweak interactions with $Z$ bosons, the production rate does not depend upon the left or right nature of the sbottom since the QCD interactions to the gluons are blind to these details. On the other hand, the sbottom–bottom–neutralino vertex is sensitive to the relative content of mass eigenstates in terms of left and right states which by its turn depend upon the mass spectrum. As we have pointed out in the Section III the lightest

sbottom is almost entirely a left state in the S5 mass spectrum, while it is an equal mixture of left and right states in the L1 mass spectrum. As can be seen in the Figs. 5 and 6, it seems plausible to conclude that the distributions are not sensitive to the particular mixtures of left and right states of the sbottom mass eigenstates, however a more detailed study including more test points is necessary to confirm this indication.

## V. CONCLUSIONS

In the near future the LHC will start its endeavor in searching for new physics signals. Once those signals have been identified as the production of new states the next logical step will be the determination of the underlying model among all candidates by measuring the properties and interactions of the new particles. The size of production cross sections and mass spectra might provide valuable hints about the underlying model, nevertheless, an undisputed discrimination will only be possible after determination of the spins of the new states. We showed that the discrimination between a SUSY spin interpretation against an UED one is possible in the case of scalar bottom (fermionic KK bottom) pair production in the reaction $pp \to b\bar{b}\not{p}_T$. Using the variable proposed in Ref. [5], see Eq. (11), we demonstrated that a clear determination of the spin of the decaying strongly interacting particle is possible provided the production cross sections and branching ratios into $b\tilde{\chi}_1^0$ are sufficiently large.Even in the worst scenario studied, the SPS1a spectrum, the determination of spins might be possible after background subtraction, however, a dedicated study of the impact of statistical and systematic errors on the spin determinations will be necessary in this test point.

[1] For reviews of SUSY, see *e.g.* : I. J. R. Aitchison, hep-ph/0505105; S. P. Martin, hep-ph/9709356.

[2] S. Dawson, E. Eichten and C. Quigg, Phys. Rev. D **31**, 1581 (1985).

[3] W. Beenakker, R. Höpker, M. Spira and P. M. Zerwas, Nucl. Phys. B **492**, 51 (1997); T. Plehn, arXiv:hep-ph/9809319; W. Beenakker, M. Krämer, T. Plehn, M. Spira and P. M. Zerwas, Nucl. Phys. B **515**, 3 (1998); W. Beenakker, M. Klasen, M. Krämer, T. Plehn, M. Spira and P. M. Zerwas, Phys. Rev. Lett. **83**, 3780 (1999); Propspino2.0 publicly available from www.ph.ed.ac.uk/~tplehn

[4] A. J. Barr, Phys. Lett. B **596**, 205 (2004);

[5] A. J. Barr, JHEP **0602**, 042 (2006).

[6] J. M. Smillie and B. R. Webber, JHEP **0510**, 069 (2005).

[7] A. Alves, O. Eboli and T. Plehn, Phys. Rev. D **74**, 095010 (2006) [arXiv:hep-ph/0605067].

[8] T. Appelquist, H. C. Cheng and B. A. Dobrescu, Phys. Rev. D **64**, 035002 (2001); T. G. Rizzo, Phys. Rev. D **64**, 095010 (2001); D. A. Dicus, C. D. McMullen and S. Nandi, Phys. Rev. D **65**, 076007 (2002); C. Macesanu, arXiv:hep-ph/0510418; G. Burdman, B. A. Dobrescu and E. Ponton, arXiv:hep-ph/0601186; M. Battaglia, A. Datta, A. De Roeck, K. Kong and K. T. Matchev, JHEP **0507**, 033 (2005); M. Battaglia, A. K. Datta, A. De Roeck, K. Kong and K. T. Matchev, arXiv:hep-ph/0507284.

[9] H. C. Cheng, K. T. Matchev and M. Schmaltz, Phys. Rev. D **66**, 056006 (2002); A. Datta, K. Kong and K. T. Matchev, Phys. Rev. D **72**, 096006 (2005) [Erratum-ibid. D **72**, 119901 (2005)]; A. Datta, G. L. Kane and M. Toharia, arXiv:hep-ph/0510204.

[10] ATLAS detector and physics performance, Technical Design Report, section 20.2.

[11] B. C. Allanach *et al.*, Eur. Phys. J. C **25**, 113 (2002).

[12] T. Stelzer, F. Long, Comput. Phys. Commun. **81** (1994) 357; F. Maltoni and T. Stelzer, JHEP **0302**, 027 (2003).

[13] K. Hagiwara *et al.*, Phys. Rev. D **73**, 055005 (2006); G. C. Cho, K. Hagiwara, J. Kanzaki, T. Plehn, D. Rainwater and T. Stelzer, Phys. Rev. D **73**, 054002 (2006).

[14] J. Pumplin, D. R. Stump, J. Huston, H. L. Lai, P. Nadolsky and W. K. Tung, JHEP **0207**, 012 (2002) [arXiv:hep-ph/0201195].

[15] ATLAS detector and physics performance, Technical Design Report, section 17.7.2; R. Hawkings, Eur. Phys. J. C **34**, s109-s116 (2004).

[16] R. Hauser [ATLAS Collaboration], Eur. Phys. J. C **34**, 173 (2004); G. Azuelos *et al.* [ATLAS Collaboration], ATL–DAQ–2003–004.

[17] V. M. Abazov *et al.* [D0 Collaboration], Phys. Lett. B **638**, 119 (2006).